

# THE OBJECT ORIENTED PARALLEL ACCELERATOR LIBRARY (OPAL), DESIGN, IMPLEMENTATION AND APPLICATION

A. Adelman\*, Ch. Kraus, Y. Ineichen, PSI, Villigen Switzerland  
 S. Russell, LANL, Los Alamos, USA,  
 Y. Bi, J.J Yang, CIAE, Beijing, China

## Abstract

OPAL (Object Oriented Parallel Accelerator Library) is a tool for charged-particle optic calculations in accelerator structures and beam lines including 3D space charge, short range wake-fields and 1D coherent synchrotron radiation and particle matter interaction. Built from first principles as a parallel application, OPAL admits simulations of any scale, from the laptop to the largest High Performance Computing (HPC) clusters available today. Simulations, in particular HPC simulations, form the third pillar of science, complementing theory and experiment. OPAL has a fast FFT based direct solver and an iterative solver, able to handle efficiently exact boundary conditions on complex geometries. We present timings of OPAL-T using the FFT based space charge solver with up to several thousands of cores.

## OPAL IN A NUTSHELL

OPAL is a tool for charged-particle optics in accelerator structures and beam lines. Using the MAD language with extensions, OPAL is derived from MAD9P and is based on the CLASSIC class library, which was started in 1995 by an international collaboration. The Independent Parallel Particle Layer ( $IP^2L$ ) is the framework which provides parallel particles and fields using data parallel ansatz, together with Trilinos for linear solvers and preconditioners. Parallel input/output is provided by H5Part/Block a special purpose API on top of HDF5. For some special numerical algorithms we use the Gnu Scientific Library (GSL).

OPAL is built from the ground up as a parallel application exemplifying the fact that HPC (High Performance Computing) is the third leg of science, complementing theory and experiment. HPC is now made possible through the increasingly sophisticated mathematical models and evolving computer power available on the desktop and in super computer centres. OPAL runs on your laptop as well as on the largest HPC clusters available today.

The state-of-the-art software design philosophy based on design patterns, makes it easy to add new features into OPAL, in the form of new C++ classes. Figure 1 presents a more detailed view into the complex architecture of OPAL.

OPAL comes in the following flavors:

- OPAL-T
- OPAL-CYCL

\* andreas.adelmann@psi.ch

[Computer Codes \(Design, Simulation, Field Calculation\)](#)

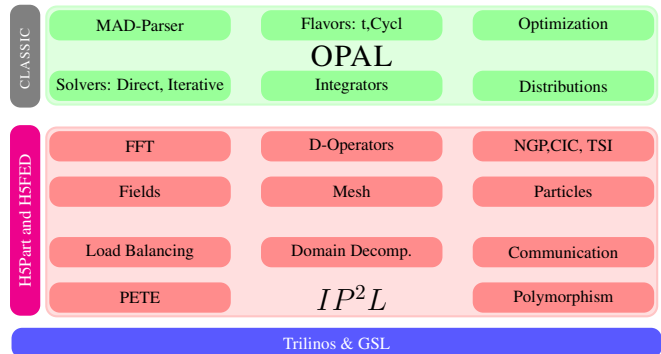


Figure 1: The OPAL software structure

- OPAL-MAP (not yet fully released)
- OPAL-ENVELOPE (not yet fully released)

OPAL-T tracks particles with time as the independent variable and can be used to model beam lines, dc guns, photo guns and complete XFEL's excluding the undulator. Collective effects such as space charge (3D solver), coherent synchrotron radiation (1D solver) and longitudinal and transverse wake fields are considered. When comparing simulation results to measured data, collimators (at the moment without secondary effects) and pepper pot elements are important devices. OPAL-CYCL is another flavor which tracks particles with 3D space charge including neighboring turns in cyclotrons, with time as the independent variable. Both flavors can be used in sequence, hence full start-to-end cyclotron simulations are possible. OPAL-MAP tracks particles with 3D space charge using split operator techniques. OPAL-ENVELOPE is based on the 3D-envelope equation (à la HOMDYN) and can be used to design XFEL's

Documentation and quality assurance are given our highest attention since we are convinced that adequate documentation is a key factor in the usefulness of a code like OPAL to study present and future particle accelerators. Using tools such as a source code version control system (subversion), and source code documentation (Doxygen) together with an extensive user manual we are committed to provide users as well as co-developers with state-of-the-art documentation for OPAL. Rigorous quality control is realized by means of daily build and regression tests.

In the sequel we will only discuss features of OPAL-T based on the current production version 1.1.5.

## MODELS

In recent years, precise beam dynamics simulations in the design of high-current low-energy hadron machines as well as of 4th generation light sources have become a very important research topic. Hadron machines are characterized by high currents and hence require excellent control of beam losses and/or keeping the emittance of the beam in narrow ranges. This is a challenging problem which requires the accurate modeling of the dynamics of a large ensemble of macro or real particles subject to complicated external focusing, accelerating fields and wake fields, particle-matter interaction, as well as the self-fields caused by Coulomb interaction of the particles. In general the geometries of particle accelerators are large and complicated which has a direct impact on the numerical solution method.

Some of the effects can be studied by using a low dimensional model, i.e., envelope equations [1, 2, 3, 4]. These are a set of ordinary differential equations for the second-order moments of a time-dependent particle distribution. They can be calculated fast, however the level of detail is mostly not sufficient for quantitative studies. Furthermore, a priori knowledge of critical beam parameters such as the emittance is required with the consequence that the envelope equations cannot be used as a self-consistent method.

One way to overcome these limitations is by considering the Vlasov-Poisson description of the phase space, including external fields and self-fields and, if needed, other effects such as wakes. To that end let  $f(\mathbf{x}, \mathbf{v}, t)$  be the density of the particles in the phase space, i.e., the position-velocity  $(\mathbf{x}, \mathbf{v})$  space. Its evolution is determined by the collisionless *Vlasov equation*,

$$\frac{df}{dt} = \partial_t f + \mathbf{v} \cdot \nabla_{\mathbf{x}} f + \frac{q}{m_0} (\mathbf{E} + \mathbf{v} \times \mathbf{B}) \cdot \nabla_{\mathbf{v}} f = 0, \quad (1)$$

where  $m_0$ ,  $q$  denote particle mass and charge, respectively. The electric and magnetic fields  $\mathbf{E}$  and  $\mathbf{B}$  are superpositions of external fields and self-fields (space charge),

$$\mathbf{E} = \mathbf{E}_{\text{ext}} + \mathbf{E}_{\text{self}} + \mathbf{E}_{\text{wake}}, \quad \mathbf{B} = \mathbf{B}_{\text{ext}} + \mathbf{B}_{\text{self}}. \quad (2)$$

If  $\mathbf{E}$  and  $\mathbf{B}$  are known, then each particle can be propagated according to the equation of motion for charged particles in an electromagnetic field,

$$\frac{d\mathbf{x}(t)}{dt} = \mathbf{v}, \quad \frac{d\mathbf{v}(t)}{dt} = \frac{q}{m_0} (\mathbf{E} + \mathbf{v} \times \mathbf{B}).$$

After the movement of the particles  $\mathbf{E}_{\text{self}}$  and  $\mathbf{B}_{\text{self}}$  have to be updated. To that end we change the coordinate system into one moving with the particles. By means of the appropriate *Lorentz transformation* [5] we arrive at a (quasi-) static approximation of the system in which the transformed magnetic field becomes negligible,  $\hat{\mathbf{B}} \approx 0$ . The

**Computer Codes (Design, Simulation, Field Calculation)**

transformed electric field is obtained from

$$\hat{\mathbf{E}} = \hat{\mathbf{E}}_{\text{self}} = -\nabla \hat{\phi}, \quad (3)$$

where the electrostatic potential  $\hat{\phi}$  is the solution of the *Poisson problem*

$$-\Delta \hat{\phi}(\mathbf{x}) = \frac{\hat{\rho}(\mathbf{x})}{\varepsilon_0}, \quad (4)$$

equipped with appropriate boundary conditions. Here,  $\hat{\rho}$  denotes the spatial charge density and  $\varepsilon_0$  is the dielectric constant. By means of the inverse Lorentz transformation the electric field  $\hat{\mathbf{E}}$  can then be transformed back to yield both the electric and the magnetic fields in (2).

In OPAL the discretized Poisson equation is either solved by a combination of a Green function and FFT or by a conjugate gradient algorithm, preconditioned with algebraic multi-grid using smoothed aggregation (SA-AMG PCG). This 3D solver has the unique capability to include the exact boundary geometry. The right hand side in (4) is discretized by sampling the particles at the grid points. In (3),  $\hat{\phi}$  is interpolated at the particle positions from its values at the grid points. We also note that the FFT-based Poisson solvers and similar approaches [6, 7] are usually restricted to box-shaped or open domains in order to obtain good performance.

### Field Solver

**A Direct FFT Based Poisson Solver** In our implementation of the PIC method, firstly a rectangular 3D grid containing all particles is constructed. Subsequently, the charges are interpolated onto the grid points. Then the discretized Poisson equation is solved on the grid to obtain the scalar field at the grid points. The electric field is calculated on the grid and interpolated back on to the positions of the particles.

In 3D Cartesian coordinates, the solution of the Poisson equation at point  $\mathbf{x}$  can be expressed by

$$\phi(\mathbf{x}) = \frac{1}{4\pi\varepsilon_0} \int G(\mathbf{x}, \mathbf{x}') \rho(\mathbf{x}, \mathbf{x}') d\mathbf{x}' \quad (5)$$

with  $G$  the 3D Green function

$$G(\mathbf{x}, \mathbf{x}') = \frac{1}{\sqrt{(\mathbf{x} - \mathbf{x}')^2}} \quad (6)$$

assuming open boundary conditions. The typical steps of calculating space charge fields using Hockney's FFT algorithm is sketched in Algorithm 1, where the quantities with superscript  $D$  (discrete) refer to grid quantities.

The image charge of a beam near a cathode is not negligible, hence open boundary conditions are not justified in such a case. To find the space-charge forces on the beam from the image charge by the standard Green function method, we need to solve the Poisson equation with a computational domain containing both the image charge and the beam. We are using a shifted-Green function [8]

**Algorithm 1** 3D Space Charge Calculation

- 1: **procedure** 3DSpaceCharge(In:  $\rho$ ,  $G$ , Out:  $\mathbf{E}_{sc}, \mathbf{B}_{sc}$ )
- 2: Create 3D rectangular grid which contains all particles,
- 3: Interpolate the charge  $q$  of each macro-particle to nearby mesh points to obtain  $\rho^D$ ,
- 4: Lorentz transformation to obtain  $\rho^D$  in the beam rest frame  $\mathbf{S}_{beam}$ ,
- 5: FFT  $\rho^D$  and  $G^D$  to obtain  $\hat{\rho}^D$  and  $\hat{G}^D$ ,
- 6: Determine  $\hat{\phi}^D$  on the grid using  $\hat{\phi}^D = \hat{\rho}^D \cdot \hat{G}^D$ ,
- 7: Use  $\text{FFT}^{-1}$  of  $\hat{\phi}^D$  to obtain  $\phi^D$ ,
- 8: Compute  $\mathbf{E}^D = -\nabla\phi^D$ ,
- 9: Interpolate  $\mathbf{E}$  at the particle positions  $\mathbf{x}$  from  $\mathbf{E}^D$ ,
- 10: Perform Lorentz back transform to obtain  $\mathbf{E}_{sc}$  and  $\mathbf{B}_{sc}$  in frame  $\mathbf{S}_{local}$  and transform back to  $\mathbf{S}_{lab}$ .
- 11: **end procedure**

technique in order to efficiently compute the correct potential at the cathode. With this technique, the FFT is used to calculate the cyclic convolution and the previous algorithm can be used to calculate the potential in the shifted field domain.

At emission from a dc gun, or when calculating neighboring turns in a cyclotron, the electrostatic approximation is not valid anymore. To overcome this problem we divide the beam into  $n$  energy bins. The space charge solver uses now  $n$  separate Lorentz transformations.

To show the parallel performance of OPAL-T we consider two problems, the first one has  $5 \cdot 10^6$  particles on a  $64 \times 64 \times 128$  mesh and 200 time steps are considered. The used CPU time as a function of cores is shown in Figure 2. We obtain in the order of  $5 \cdot 10^6$  particle pushes per second on a 16 nodes (HP BL460c blades) cluster, each node having a dual-socket quad core Intel Xeon E5450 3.0 GHz with 16GB ECC RAM. For a high-bandwidth low-latency communication the InfiniBand interconnect is used.

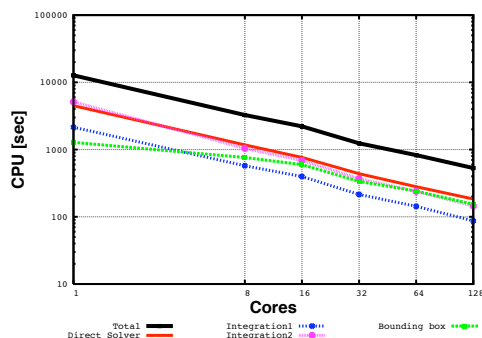


Figure 2: CPU time of a production run showing the scaling of the most important parts of OPAL-T on a 128 core HP Cluster.

The second problem consists of  $1 \cdot 10^8$  particles on a  $512^3$  mesh and timings for 3 integration steps are shown in Figure 3. The timings were obtained on the Cray XT5 cluster of the Swiss Supercomputing Center (CSCS) in Manno. Each of the 1844 compute nodes consists of 2 quad-core AMD Opteron 2.4 GHz Shanghai processors giving 8 cores in total per node with 16 GBytes of memory. The high-speed network based on a SeaStar 2.2 communications processor which is able to provide 2 GBytes/s of injection bandwidth for the node, with a theoretical peak of 9.6 GBytes/s of bandwidth in each direction for the through-flow of packets out on the network.

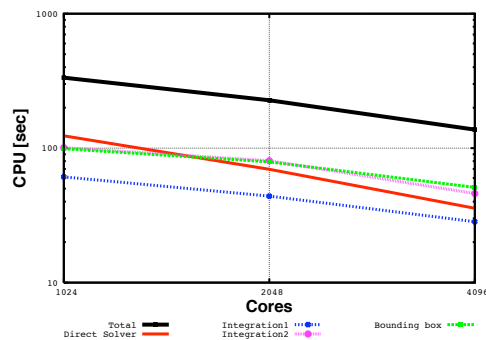


Figure 3: CPU time of a test run showing the scaling of the most important parts of OPAL-T on a Cray XT5.

**A Fast Iterative Parallel Poisson Solver on Irregular Domains** The problem is discretized by finite differences. Depending on the treatment of the Dirichlet boundary the resulting system of equations is symmetric or ‘mildly’ nonsymmetric positive definite. In all cases, the system is solved by the preconditioned conjugate gradient algorithm with smoothed aggregation (SA) based algebraic multigrid (AMG) preconditioning. Additionally we investigated variants of the implementation of SA-AMG that lead to considerable improvements in the execution times. We demonstrate good scalability of the solver on distributed memory parallel processor with up to 2048 processors in [9]. In this paper we also compare our SAAMG-PCG solver with the FFT-based solver described in the preceding paragraph.

### Particle Matter Interaction

The physics models describing particle matter interaction includes energy loss and Coulomb scattering. The nuclear scattering is not yet included for particles in the order of hundreds of MeVs. Their contribution is negligible compared to Coulomb scattering. The energy loss model is based on the Bethe-Bloch equation. Comparing the stopping power with the PSTAR program of National Institute of Standards and Technology (NIST), we find errors in the order of 10% for copper, from several MeV to 10 GeV. Important for our immediate application at PSI, the error is within 3% in the region from 50 MeV to 1 GeV. In general, there is energy straggling when a beam passes through

the material. For relatively thick absorbers such that the number of collisions is large, the energy loss distribution is Gaussian [10]. The Coulomb scattering is treated as two independent events: the multiple Coulomb scattering and the large angle Rutherford scattering, using the distribution given in [11].

**Validation** A 72 MeV cold Gaussian beam with  $\sigma_x = \sigma_y = 5$  mm is sent through a copper slit with the half aperture of 3 mm from 0.01 to 0.1 m. Figure 4 shows some trajectories of particles which are either absorbed or deflected by the collimator. Most of the particles were absorbed

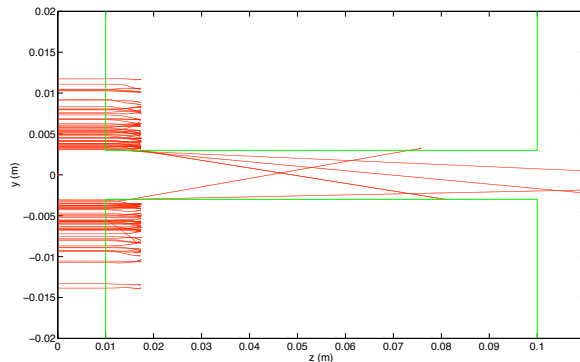


Figure 4: Trajectories of particles which are either absorbed or deflected by the collimator.

within a range of about 7.4 mm, except for a few which were deflected by the collimator. As a benchmark of the elliptic collimator models in OPAL, the energy spectrum and angle deviation is compared against two general-purpose Monte Carlo codes, MCNPX [12] and FLUKA [13, 14], as shown in Fig. 5. The deflected particles contribute to the energy spectrum and angle deviation after a collimator. These particles may be lost downstream.

## ACKNOWLEDGMENTS

The majority of computations have been performed on the Cray XT5 in the framework of the PSI CSCS “Horizon” collaboration. We acknowledge the help of the XT5 support team at CSCS, most notably Timothy Stitt and D. Kiselev for the MCNPX simulations and fruitful discussions w.r.t. the particle matter interaction models.

## REFERENCES

- [1] Frank James Sacherer. *Transverse Space-Charge Effects in Circular Accelerators*. PhD thesis, University of California, Berkeley, 1968.
- [2] Frank J. Sacherer. RMS envelope equations with space charge. *IEEE Trans. Nucl. Sci.*, 18(3):1105–1107, 1971.
- [3] J. Struckmeier and M. Reiser. Theoretical studies of envelope oscillations and instabilities of mismatched intense

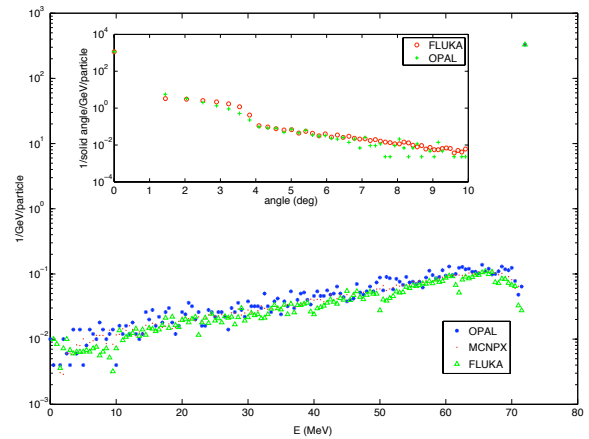


Figure 5: Energy spectrum and angle deviation (small plot)

charged-particle beams in periodic focusing channels. *Part. Accel.*, 14(2-3):227–260, 1984.

- [4] R. L. Gluckstern. Analytic model for halo formation in high current ion linacs. *Phys. Rev. Lett.*, 73(9):1247–1250, 1994.
- [5] L. D. Landau and E. M. Lifshitz. *Electrodynamics of Continuous Media*. Pergamon, Oxford, 2nd edition, 1984.
- [6] Ji Qiang and Robert D. Ryne. Parallel 3D Poisson solver for a charged beam in a conducting pipe. *Comp. Phys. Comm.*, 138(1):18–28, 2001.
- [7] Ji Qiang and Robert L. Gluckstern. Three-dimensional Poisson solver for a charged beam with large aspect ratio in a conducting pipe. *Comp. Phys. Comm.*, 160(2):120–128, 2004.
- [8] Ji Qiang, Steve Lidia, and Robert D Ryne. Three-dimensional quasistatic model for high brightness beam dynamics simulation. *Phys. Rev. ST Accel. Beams*, 9(4):1–10, Apr 2006.
- [9] A Adelman, P Arbenz, and Y Ineichen. A fast parallel poisson solver on irregular domains applied to beam dynamic simulations. *arXiv*, physics.comp-ph, July 2009.
- [10] William R. Leo. *Techniques for nuclear and particle physics experiments*. Springer-Verlag, Berlin Heidelberg New York, 2nd edition, 1994.
- [11] J. D. Jackson. *Classical Electrodynamics*. John Wiley & Sons, New York, 3rd edition, 1998.
- [12] D. Pelowitz ed. MCNPX Users Manual. Technical Report Version 2.5.0 LA-CP-05-0369.
- [13] G. Battistoni, S. Muraro, P.R. Sala, F. Cerutti, A. Ferrari, S. Roesler, A. Fasso, and J. Ranft. The fluka code: Description and benchmarking. In *Proceedings of the Hadronic Shower Simulation Workshop 2006*, Fermilab, 2006. M. Albrow, R. Raja eds., AIP Conference Proceeding 896, 31-49, (2007).
- [14] A. Fasso, A. Ferrari, J. Ranft, and P.R. Sala. Fluka: a multi-particle transport code. Tech. Report CERN-2005-10 (2005), INFN/TC.05/11, SLAC-R-773, 2005.